Modeling the interactions between peptide functions and Sr2+: Formamide-Sr2+ reactions in the Gas Phase

Ane Eizaguirre, Otilia Mó, Manuel Yáñez, Jean-Yves Salpin

Modeling the interactions between peptide functions and Sr^{2+}: Formamide-Sr^{2+} reactions in the Gas Phase

Ane Eizaguirre[1], Otília Mó[1], Manuel Yáñez[1], Jean-Yves Salpin[2,3]

[1]*Departamento de Química, Módulo 13, Facultad de Ciencias. Universidad Autónoma de Madrid. Campus de Excelencia UAM-CSIC. Cantoblanco. 28049 – Madrid. Spain*

[2]*Université d'Evry Val d'Essonne – Laboratoire Analyse et Modélisation pour la Biologie et l'Environnement (LAMBE) – Bâtiment Maupertuis – Boulevard François Mitterrand, 91025 Evry, France*

[3]*CNRS – UMR 8587*

Abstract

The interactions between formamide, which can be considered a prototype of a peptide function, and Sr^{2+} have been investigated by combining nanoelectrospray ionization/mass spectrometry techniques and G96LYP DFT calculations. For Sr an extended LANL2DZ basis set was employed, together with a 6-311+G(3df,2p) basis set expansion for the remaining atoms of the system. The observed reactivity seems to be dominated by the Coulomb explosion process yielding $[SrOH]^+ + [HNCH]^+$, which are the most intense peaks in the MS/MS spectra. Nevertheless, additional peaks corresponding to the loss of HNC and CO indicate that the association of Sr^{2+} to water or to ammonia leads to long-lived doubly charged species detectable in the timescale of these experimental techniques. The topology of the calculated potential energy surface permits to establish the mechanisms behind these processes. Although the interaction between the neutral base and Sr^{2+} is essentially electrostatic, the polarization triggered by the doubly charged metal ion results in the activation of several bonds, and favors different proton transfer mechanisms required for the formation of the $[SrOH]^+$, $[SrOH_2]^{2+}$ and $[SrNH_3]^{2+}$ products.

Introduction

Up to recent years, molecular dications, ML^{2+} formed by the association of neutral chemical compounds and doubly charged metal ions were oddities, due to the difficulty of generating them in the gas phase. These difficulties are particularly severe for transition metals having rather high second ionization energies. Most often in those cases, the only ions experimentally detectable are singly charged $[M(L-H)]^+$ species,[1-5] in which the neutral ligand has lost a proton. This is not the case however for alkaline-earth metals, such as Ca, Sr or Ba, which have much smaller second ionization energies and yield easily detectable ML^{2+} dications[6-14] and whose unimolecular reactivity upon collision could be explored.[6-8, 10] In these cases, some of the observed fragmentations correspond to the loss of a neutral fragment L', which turns out to be an effective way of producing lighter doubly charged molecular ions, such as $[CaNH_3]^{2+}$.[6, 8, 10]The aim of this paper is to present a combined theoretical and experimental study on the unimolecular reactivity of the doubly charged ions formed by the interaction of formamide ($HCONH_2$), as the simplest prototype of a peptide function[15-20] and Sr^{2+}. Besides, the formamide molecule seems to have played also a relevant role in the early earth chemistry.[21] Although the composition of the early earth and its atmosphere is still matter of debate, it is believed that its elemental and molecular composition is represented in the comets and asteroidal bodies still circulating in the Solar System.[21] Their composition reveals that formamide, together with cyanhydric acid (HCN), isocyanate (HNCO) and water (H_2O), constitute the most abundant molecules containing the four biologically relevant elements, O, N, H and C.[22-24] Hence, formamide seems to play a positive role as a synthon for purine and pyrimidine nucleobases acting as a prebiotic precursor.[25-28] The efficiency of formamide chemistry in the origin of the informational polymers strictly depends on the metal oxides and minerals used in its condensation.[29]

The reactivity of this molecule has also attracted much attention because it constitutes a suitable model to study the reactivity of larger biochemical compounds.[15-20] In particular, formamide-formamidic acid tautomerization has been used to model the tautomerization of larger bases such as guanine and uracil systems.[30-33] This tautomerization process has been also studied for protonated formamide and formamide-X^+ (X = Li, Na, Mg and Al).[34] Also interestingly, the formamide moiety is the simplest amide containing a prototype HNC=O peptide linkage and can be used as a model to understand proton exchange processes in peptides and proteins[35] or the hydrolysis of peptide bonds[36] in living systems. In order to study how does influence the metal interaction in the fragmentation of the formamide, the reactivity of the [Cu-Formamide]$^+$ and [Ni-Formamide]$^+$ systems has been studied from the theoretical and the experimental points of view.[37, 38]

Strontium has shown to provide an electrostatic interaction when attached to uracil molecule.[39] Considering the zwitterionic resonant form of formamide[40] structure it could be expected that a strong ion-dipole interaction could exist between them. Also interestingly, the bivalent character of the Sr^{2+} dication allows the investigation of the Coulomb explosions in this system. For these purposes we have used electrospray ionization/mass spectrometry techniques. These techniques have opened up the possibility of producing clusters involving metal dications in the gas phase from aqueous solution[41] and therefore of gaining direct information about the intrinsic reactivity of organic molecules when interacting with metal dications. In order to obtain a more detailed picture of the reactivity patterns we have also postulated an appropriate reaction mechanism based on the topology of the potential energy surface of the Sr^{2+}/formamide system.

Experimental and Computational Details

Experimental section

Electrospray MS/MS mass spectra were recorded on a QSTAR PULSAR i (Applied Biosystems/MDS Sciex) hybrid instrument (QqTOF) fitted with a nanospray source. Typically, 10 μL of a 1:1 aqueous mixture of strontium chloride and formamide (10^{-4} mol L^{-1}) were nanosprayed (20–50 nL/min) using borosilicate emitters (Proxeon). The sample was ionized using a 900 V nanospray needle voltage and the lowest possible nebulizing gas pressure (tens of millibars). The declustering potential DP (also referred to as "cone voltage" in other devices), defined as the difference in potentials between the orifice plate and the skimmer (grounded), ranged from 0 to 120 V. The operating pressure of the curtain gas (N_2), which prevents air or solvent from entering the analyzer region, was adjusted to 0.7 bar by means of pressure sensors, as a fraction of the N_2 inlet pressure. To improve ion transmission and subsequent sensitivity during the experiments, the collision gas (CAD, N_2) was present at all times for collisional focusing in both the Q0 (ion guide preceding the quadrupole Q1 and located just after the skimmer) and Q2 (collision cell) sectors.

For MS/MS spectra, complexes of interest were mass selected using Q1, and allowed to collide with nitrogen as collision gas in the second quadrupole (Q2), the resulting product ions being analyzed by the time-of-flight (TOF) after orthogonal injection. Furthermore, MS/MS spectra were systematically recorded at various collision energies ranging from 7 eV to 22 eV in the laboratory frame (the collision energy is given by the difference between the potentials of Q0 and Q2). This corresponds to a center-of-mass collision energies (E_{CM}) ranging from 2.43 to 7.65 eV. The CAD parameter, which roughly controls the amount of N_2 introduced into Q2, was set to its minimum value in order to limit multiple ion–molecule collisions. Setting this parameter to 1 during

MS/MS experiments resulted in pressure values of 1-2 10^{-5} Torr as measured by the ion gauge located at vicinity but outside the collision cell. It has been reported that the pressure inside the collision cell is fact in the order of 10 mTorr. At this pressure and given the dimension of the LINAC collision cell (about 22 centimeters long), on can find that the mean free path for a N_2 molecule is about 5 mm. So, at this pressure not only N_2 molecule but also complexes of interest (which have higher collision cross-sections) may undergo tens of collisions along their path through Q2. Note that this estimate is a lower limit since N_2 also enters Q0 and Q1 for collisional focusing. Consequently, even with the minimum amount of N_2 inside the collision cell, we are certainly still under a multiple collision regime.

All experiments were performed in 100% water purified with a Milli-Q water purification system. Both formamide and strontium chloride were purchased from Aldrich (St Quentin-Fallavier, France) and were used without further purification. Unless otherwise noted, mass to charge ratios mentioned throughout this paper refer to as peaks including the most abundant strontium isotope (^{88}Sr).

Computational details

All the structures under study were optimized using Density Functional Theory (DFT). In particular we have used the hybrid functional G96LYP,[42,43] which in a previous assessment was found to be rather appropriate for the description of Sr^{2+} complexes.[44] This functional was used together with a 6-31+G(d,p) basis set expansion for C, N, O and H atoms and an improved LANL2DZ[44] basis set for Sr^{2+} cation. In order to ensure the reliability of the estimated stability of the different structures, the final energy of each system was obtained in single-point calculations using the 6-311+G(3df,2p) basis set expansion for C, N, O and H atoms and an extended LANL2DZ[44] for the Sr^{2+} cation.

Harmonic vibrational frequencies were obtained at the same level of theory used for geometry optimizations in order to estimate the corresponding Zero-Point Vibrational Energy (ZPVE) corrections and to classify stationary points of the Potential Energy Surface (PES) either as local minima or Transition States (TS). Sr^{2+} binding energies were evaluated by subtracting from the energy of the most stable adduct, the energy of the neutral formamide in its equilibrium conformation and that of Sr^{2+}, after including the corresponding ZPVE corrections. We have verified that the basis set superposition error (BSSE), evaluated by using the counterpoise method,[45] was always smaller than 3.5 kJ mol^{-1}, in agreement with similar funding in the literature, [46, 47] and with the fact that the BSSE for DFT calculations is usually much smaller than for post-HF *ab initio* approaches.[48, 49] All these calculations have been carried out with the Gaussian 03 suite of programs.[50]

The bonding of the most relevant structures was studied by using the atoms in molecules (AIM) theory[51, 52] which is based on a topological analysis of the electron density. This approach permits the definition of the molecular graph as the ensemble of bond critical points (BCPs) and bond paths. The BCPs are stationary points in which the electron density is minimum only in one direction, whereas the bond paths correspond to the lines that, containing the BCP, connect two neighbor maxima of the density. In general, the electron density, as well as the energy density calculated at BCPs, gives useful information on the strength and nature of the bond. These molecular graphs were obtained by means of the AIMPAC series of programs.[53]

The bonding AIM analysis was complemented with the one obtained by using the Becke and Edgecombe electron localization function (ELF).[54] This theory provides useful information about the nature of the bonding, even in challenging cases in which other approaches fail to give an unambiguous bonding picture.[55] ELF has been originally conceived as a local measure of the Fermi hole curvature around a reference

point. A Lorentz transform allows ELF to be confined in the [0,1] interval, where 1 corresponds to regions dominated by an opposite spin pair or by a single electron. In this way, the valence shell of a molecule can be described in terms of two types of basins: polysynaptic basins (generally disynaptic), with the participation of several (generally two) atomic valence shells and monosynaptic ones, which correspond to electron lone pairs or core pairs of electrons. ELF calculations were carried out with the TopMod suite of programs.[56] These analyses were completed with natural bond orbital (NBO) and natural resonance theory (NRT) calculations.[57] The former permits describing the bonding in terms of localized hybrids and lone-pairs, and the second provides the weight of the different resonant structures that contribute to the stability of a given system. For all bonding analysis, the Sadlej basis set expansion [58-61] was used due to the reliability of all electron basis sets when dealing with electron density topological analysis. These calculations have been carried out with the NBO-5G series of programs.[62]

Results and Discussion

Experimental results

The positive-ion nanospray spectrum obtained with a 1:1 aqueous mixture of strontium chloride and formamide (10^{-4} mol/L) is remarkably simple (not shown). Strontium-containing ions can be easily identified because of the specific isotopic distribution of this metal, resulting in characteristic triplets. Several types of ions are observed. Like for Ca^{2+} ions,[6-8, 63] adopting a low cone voltage (DP=0 V) results in the abundant production doubly-charged species. At DP=0V, the mass spectrum is characterized by prominent hydrated strontium ions ($[Sr(H_2O)_m]^{2+}$; m = 1–3) detected at *m/z* 52.92, 61.96 and 70.97, respectively, while strontium hydroxide $[SrOH]^+$ (*m/z*

104.90) is a minor species. The situation is reversed when increasing the declustering potential and at high DP the spectrum is dominated by $[SrOH]^+$ and $[SrOH(H_2O)]^+$ ions. Interaction between formamide and strontium ion gives rise almost exclusively to doubly-charged complexes of the type $([Sr(formamide)_n]^{2+}$.(n=1,2) observed at *m/z* 66.47 and 88.97. Singly charged complexes of general formula $[Sr(formamide)_n - H]^+$ are practically not detected, regardless of the electrospray interface conditions.

We will now focus on the MS/MS spectra of the $[Sr(formamide)]^{2+}$ complex. These spectra have been recorded at various DP values and were found not to depend on this parameter. A typical CID spectrum recorded at DP=30 V for the $[Sr(formamide)]^{2+}$ species is given in Figure 1. Note that on our instrument and for this particular system, the smallest collision energy in the laboratory frame (E_{lab}) for which sufficient amount of fragment ions can reach the detector, was 7 eV, and at this value dissociation of the precursor ions already occurs. E_{lab} was scanned from 7 to 22 eV. This corresponds to a center-of-mass collision energies (E_{CM}) ranging from 2.43 to 7.65 eV, N_2 being used as target gas. The $[Sr(formamide)]^{2+}$ complex dissociates according to either neutral losses generating new dications, or through a charge separation process leading to singly

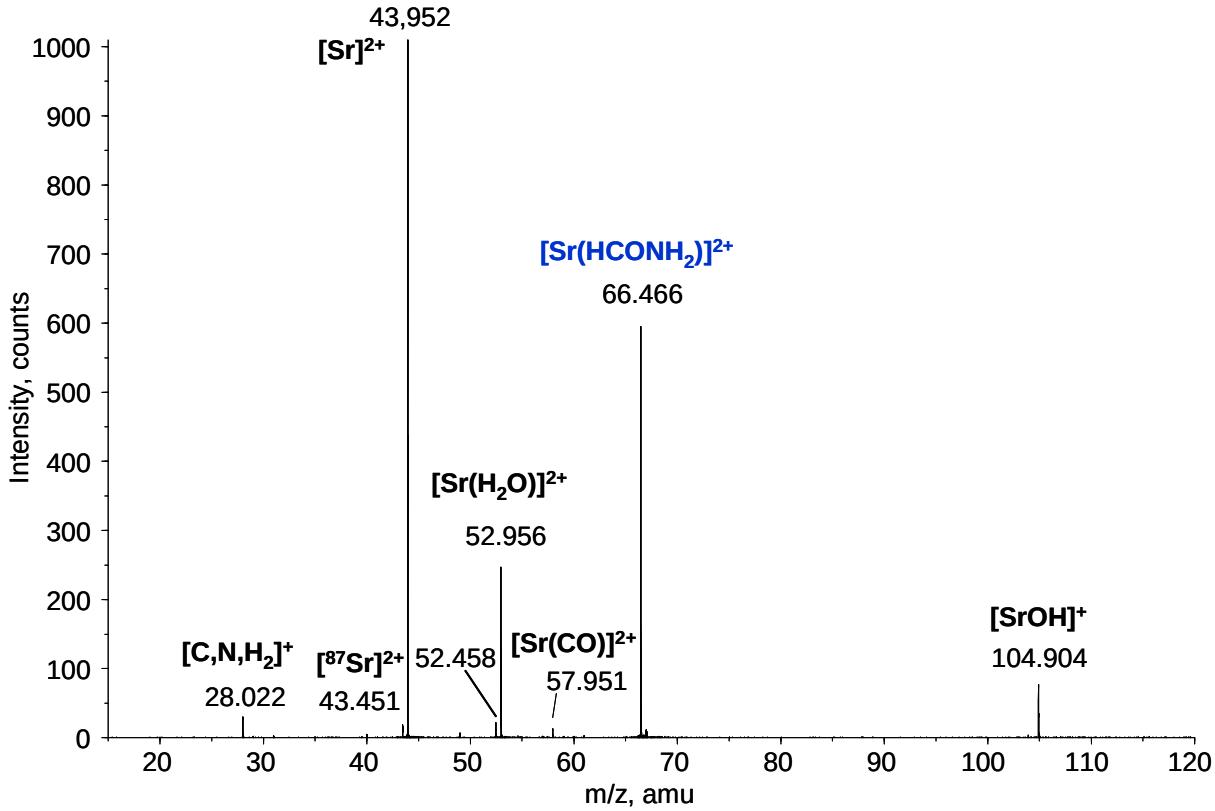

Figure 1. Low-energy MS/MS spectrum of the $[^{88}Sr(formamide)]^{2+}$ recorded at a collision energy of 11 eV (laboratory frame), the declustering potential being set at 35 V. See text for details.

charged species. At low collision energy (below 10 eV), the most intense doubly charged fragment species (*m/z* 52.96) is the $[Sr(H_2O)]^{2+}$ ion. Bare Sr^{2+} ion (*m/z* 43.95) is also detected but to a lesser extent. However, the abundance ratio of these two particular ions quickly reverses as one increases the collision energy. This might suggest that Sr^{2+} ions may arise from $[Sr(H_2O)]^{2+}$ through consecutive processes. Another doubly charged complex is also detected in low abundance at m/z 57.95 and certainly corresponds to the formation of the $[Sr,C,O]^{2+}$ ions through the elimination of a NH_3 molecule. Note that one also observes an ion at *m/z* 52.46 that could be attributed to a $[Sr(NH_3)]^{2+}$ complex. These two ions would then suggest the formation of an intermediate in which the metallic centre would interact with both ammonia and carbon monoxide. However, examination of Figure 1 shows up the presence of the $^{87}Sr^{2+}$ ion at *m/z* 43.45. Consequently, a small fraction of the ^{87}Sr isotope has been also selected

during these MS/MS experiments and therefore the *m/z* 52.46 ion could also be attributed to $[^{87}Sr(H_2O)]^{2+}$.

The last fragmentation observed onto the MS/MS spectra corresponds to a charge separation process leading to two singly charged fragment ions at m/z 28.02 and 104.90, corresponding to $[C,N,H_2]^+$ and $[SrOH]^+$, respectively. Partner peaks arising from such a process should have in principle the same intensity. However, as it was already found for the Ca^{2+}-containing systems[6-8, 63, 64] the lightest ion is less intense than the heaviest one. This phenomenon has been interpreted in terms of different radial ion energies, with the lighter ions generated by the Coulomb explosion gaining most of the radial energy and therefore having a much higher velocity than the relatively high mass ions. This can result in an unstable ion trajectory within the instrument and explains why lighter ions are detected in the MS/MS spectrum with smaller abundance.

It is also worth noting that the fragmentation upon collision of the $[Sr(formamide)]^{2+}$ appears somewhat similar to the dissociation of the $[Ni(formamide)]^+$ complex studied either under metastable or low-energy conditions. The MIKE spectrum of the $[Ni(formamide)]^+$ complex is indeed characterized by elimination of intact formamide and both losses of ammonia and water.[38] Note that elimination of ammonia was no longer observed under low-energy CID conditions. The $[Sr(formamide)]^{2+}$ complex also shares common fragmentation patterns with the singly charged ion $[Cu(formamide)]^+$,[37] such as elimination of ammonia, [H,C,N], or formation of bare metal ion. On the other hand, both dehydrogenation and dehydration are exclusively observed with the transition metals.

Characteristics of $[Formamide\text{-}Sr]^{2+}$ Complexes. The most relevant features of the formamide-Sr^{2+} PES, provide a rationale to the experimental findings outlined in the previous section. The optimized geometries for the formamide-Sr^{2+} adduct (**1**) and the

most relevant stationary points of the corresponding PES are presented in Figure 2. Their total energies and the ZPVE corrections are given in table S1 of the supporting information.

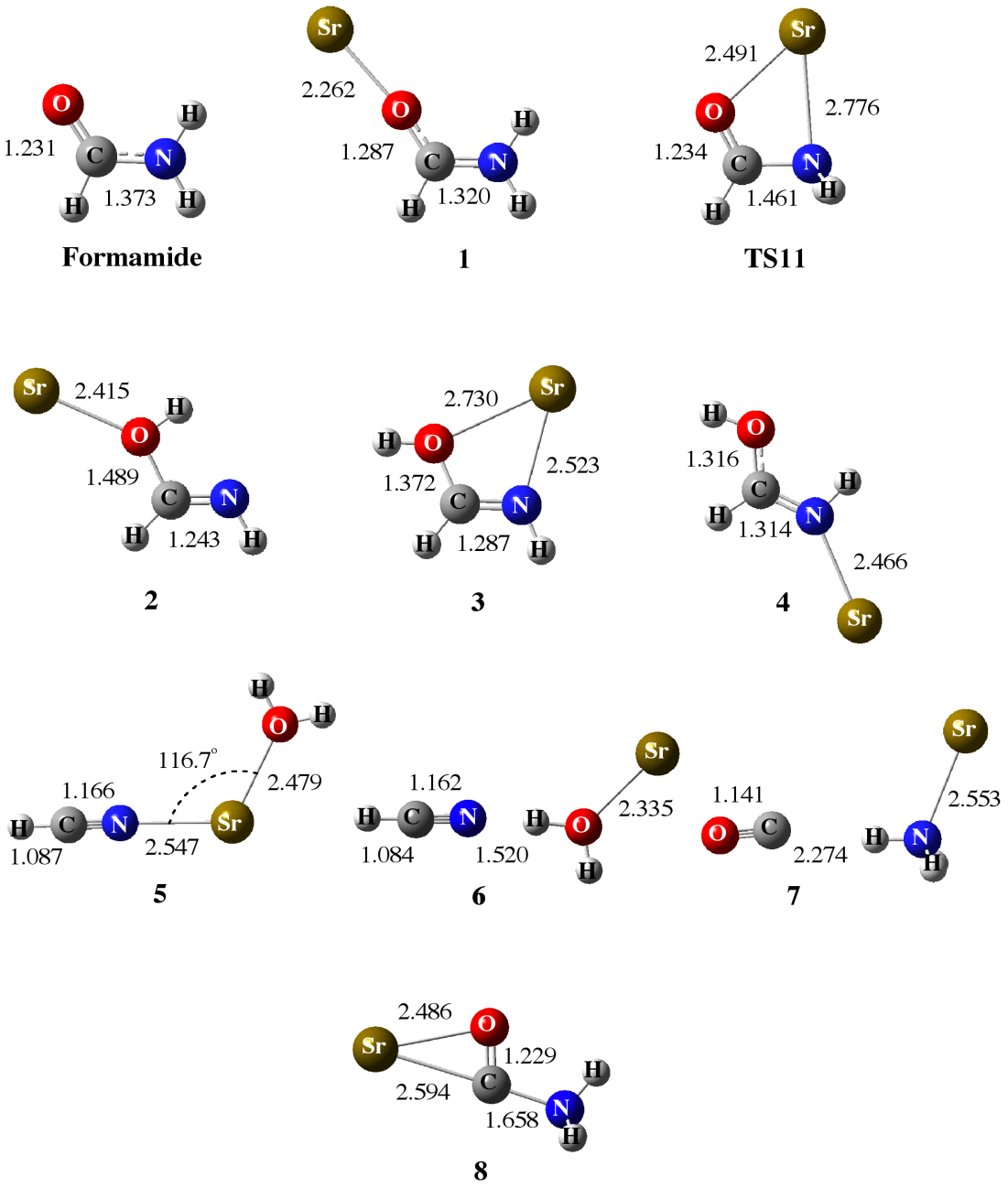

Figure 2. Optimized geometries for formamide and $[Sr\text{-Formamide}]^{2+}$ complexes. Bond lengths are in Angströms, and bond angles in degrees.

The most stable structure, **1**, of the $[C,N,O,H_3,Sr]^{2+}$ complexes corresponds to the direct association of the Sr^{2+} cation to the carbonyl oxygen of formamide. This is similar to

what has been found before for formamide-X (X = Li^+, Na^+, Mg^+, Al^+) systems,[34] but at variance with the behavior observed with transition metal ions, such as Cu^+ or Ni^+, where besides the adduct in which the metal attaches to the carbonyl group, the adduct to the amino group is also a local minimum of the PES.[37, 38] Furthermore, whereas in complex **1** the C=O—Sr^{2+} fragment is practically linear, the C=O—Cu^+ one in the corresponding Cu^+ adduct is bent,[37] the C=O—Cu^+ angle being 132.6 degrees. Consistently, whereas for the formamide-Sr^{2+} adduct only one conformation is observed in the case of Cu^+ adducts two conformers, *cis* and *trans* to the amino group, are stable. These differences are a clear consequence of the non-negligible covalent contributions to the formamide-Cu^+ interactions, whereas when dealing with Sr^{2+} these interactions are essentially electrostatic (*vide infra*). All attempts to locate a minimum in which the metal is attached to the N atom collapsed to complex **1**, or to the transition state, **TS11**, in which the metal interacts simultaneously with both basic sites. The remaining local minima of the PES are obtained from minimum **1** trough appropriate hydrogen shifts.

The interaction between formamide and Sr^{2+} can be easily understood by taking into account the dipole character of neutral formamide, which has already been highlighted in the literature,[40] which partially arises from the non negligible participation of the zwitterionic resonant structure **b**, shown in Scheme 1.

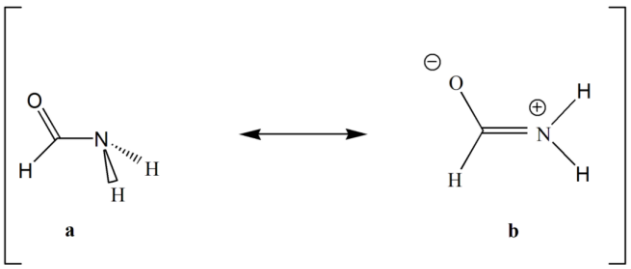

Scheme 1

As a matter of fact the weight of this zwitterionic form, obtained through the use of the NRT is quite significant (See Table 1). Hence, a strong electrostatic interaction of the molecule with the doubly charged metal ion should be expected, in coherence with the

topological analysis of the charge density of the complex **1**, which shows that the electron density at the O—Sr^{2+} BCP is rather small and the Laplacian of the charge density positive. Also consistently, the ELF plot for complex **1** does not contain any O—Sr^{2+} disynaptic basin for bond (See Figure 3), corroborating the electrostatic character of the interaction. However, the strong polarization of the base caused by the metal dication increases the conjugation of the amino group in complex **1**. This effect is clearly mirrored in the greater participation of the zwitterionic form (**b**) (see Table 1), in the planarity of the system, and in the electron density redistributions revealed by the topological analysis of the charge density shown in Figure 3. It is evident, that whereas in formamide there is a monosynaptic basin on the N atom, associated with the N lone-pair, in complex **1** it forms part of the disynaptic C-N basin. This conjugation is obviously reflected in a shortening of the C-N bond (see Figure 2) and in an increase of the electron density at the C-N BCP (See Figure 3). Concomitantly, the greater participation of the zwitterionic form **b** leads to a lengthening of the C=O bond, which partially loses its double bond character, and to a decrease of the electron density at the C—O BCP.

Table 1. Weight of the resonant forms shown in Scheme 1 for neutral formamide and the formamide adduct, **1** and the transition state, TS11, obtained by natural resonance theory calculations.

	a	**b**
Fomamide	60%	30%
1	30%	56%
TS11	88 %	

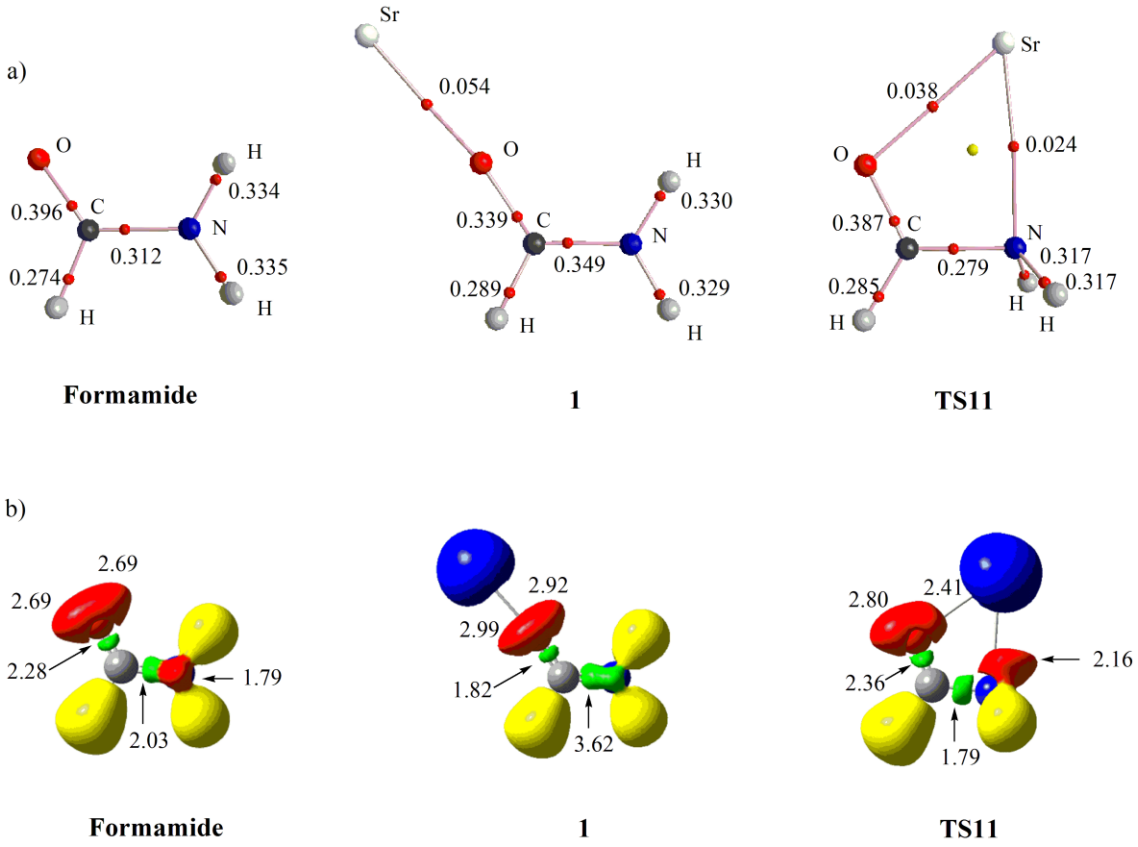

Figure 3. a) Molecular graph of neutral formamide and, **1** and **TS11** $[Sr(Formamide)]^{2+}$ complexes. Electron densities at BCP are in a.u. b) Three dimensional representation of ELF isosurface with ELF = 0.8 for neutral formamide and, 1 and TS11 $[Sr(Formamide)]^{2+}$ complexes. Yellow lobes corresponds to V(C,H) and V(N,H) basins, red lobes corresponds to V(N) and V(O) basins associated with N and O lone-pairs respectively. Green lobes correspond to V(C,C), V(C,N) and V(C,O) basins. Blue lobes correspond to Sr metal core. The population of the different basins are also indicated.

Remarkably, the stationary point **TS11** connects the global minimum **1** with itself, in a kind of circular orbiting of the metal cation, which is illustrated in Figure 4. When the metal dication is attached to the carbonyl oxygen the system is stabilized by the aforementioned greater participation of the zwitterionic form **b**, which favors a stronger electrostatic interaction between the metal and carbonyl oxygen. The migration of the metal towards the amino group has to surmount a significant activation barrier due primarily to the electrostatic repulsion between the positive charges on Sr and on the NH_2 group, which favors the coming back of the metal to its original position (see

Figure 4). We have estimated this repulsion to account for 70 kJ mol^{-1} of the activation barrier. The remaining energy required to reach **TS11**, another 70 kJ mol^{-1}, is associated with the necessary pyramidalization of the amino group, which is clearly reflected in a very large participation of the resonant form **a**, which in **TS11**, becomes dominant. Consistently, on going from **1** to **TS11**, C—O and the C—N bonds significantly shorten and lengthen, respectively (See Figure 2) and the electron densities at the corresponding BCPs, as well as the populations of the corresponding disynaptic basins increase and decrease also significantly (see Figure 3).

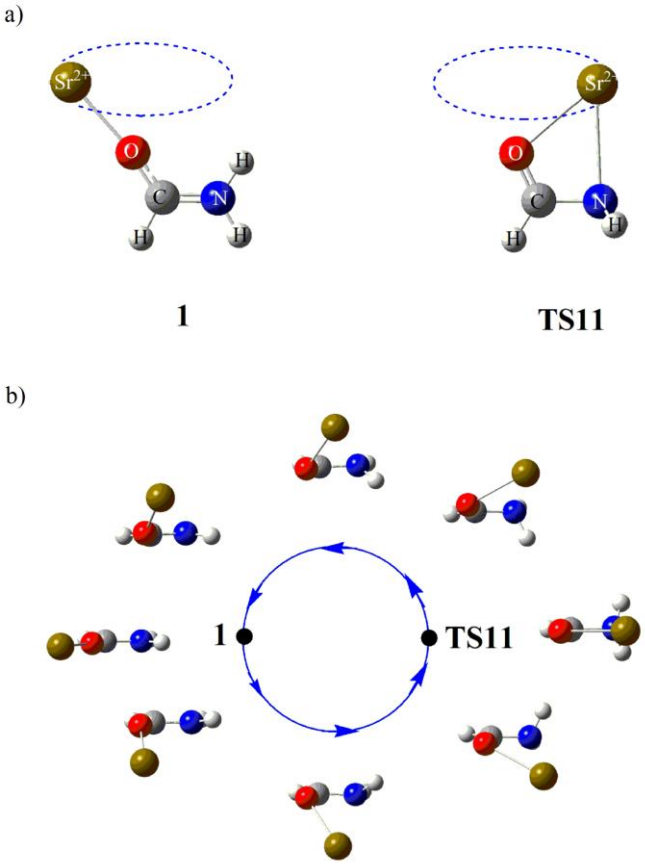

Figure 4. a) The circular orbit composed by minimum **1** and **TS11**.b) The top view of the circular orbit described by Sr^{2+} in complex **1** on going through **TS11**.

It is worth mentioning that other orbital rearrangements have been reported previously in the literature.[65, 66] However, in those cases the origin of the orbiting described for the

metal was essentially due to the high symmetry of the system and involved very low activation barriers, whereas in the case discussed here the origin is associated with the dipole character of the formamide moiety, and involves rather high activation barriers. Also interestingly, the same orbital rearrangement was not found for the [Formamide-$Cu]^+$ and [Formamide-$Ni]^+$ systems.[37, 38] As mentioned above, in these cases the non negligible covalent character of the Cu^+-Formamide and Ni^+-Formamide interactions gives rise to two stable adducts, in which the metal interacts either with the carbonyl or with the amino group, and therefore the structure similar to **TS11**, in which the metal bridges between both basic sites is a transition state connecting these two adducts.

Mechanisms associated with the fragmentation upon collision induced dissociation observed for the ~~Unimolecular Reactions of~~ [Sr (Formamide)]$^{2+}$ Ions.

Schematic potential energy profiles corresponding to the unimolecular reactions of the [Sr(Formamide)]$^{2+}$ complex are shown in Figure 5. We have distinguished those mechanisms associated with the loss of a neutral fragment (black solid lines) from those corresponding to the formation of two monocations through Coulomb explosion processes (red dashed lines).

Starting from minimum **1**, three possible proton transfer reactions can be envisaged. It should be noted that the height of the barrier of these processes lies above the already discussed potential barrier **TS11**, and therefore in the three processes the approaching of the Sr^{2+} cation to the nitrogen atom is feasible. Among all of them, the most favorable process from the energetic viewpoint corresponds to the proton transfer from the NH_2 group to the oxygen atom via **TS12**, leading to the secondary local minimum, **2**. This transition state lies at 247 kJ mol^{-1} above minimum **1**. It is worth noting that the metal attachment does not catalyze the keto-enolic tautomerization, since the calculated barrier is 75 kJ mol^{-1} higher than that obtained at the same level of theory for the

tautomerization of isolated formamide. This is in contrast with the catalytic effects predicted by Ca^{2+} and by Sr^{2+} for the enolic tautomerization of uracil and its thio- and seleno-derivatives.[39, 67, 68] This can be understood if one takes into account that in uracil there are two carbonyl groups susceptible of undergoing enolization, and the catalyzed process is the one involving the carbonyl group which is not interacting with the metal dication.[39, 67, 68] For formamide, the enhanced acidity of the amino group in complex **1** is counterbalanced by the significant reduction of the basicity of the carbonyl group, whose electron density is strongly polarized towards the doubly charged metal ion. Minimum **2** may give rise to a Coulomb explosion process via **TS2A** leading to the products $[Sr\text{-}OH]^+ + [HNCH]^+$ (**A** in the PES of Figure 5a). These fragments correspond to the partner peaks observed at *m/z* 104.90 and 28.02, respectively in the MS/MS spectra. Alternatively, minimum **2** may yield structure **6** through a multi-step mechanism (See Figure 5b). This pathway involves the rotation of the Sr-OH group followed by the rotation of the NH-Sr group via **TS23** and **TS34**, respectively. Subsequently, the proton transfer from the NH to the OH group, is accompanied by the migration of the water molecule via **TS45**. Once structure **5** is formed, there are apparently two obvious mechanisms, the loss of HCN or the loss of water, the latter being energetically favored. However, much more favorable than these two bond cleavages is the evolution to yield complex **6**, since this process involves a barrier much lower than the energy required to produce the loss of hydrogen cyanide or water. Hence, very likely all flux will go to the production of **6**. From **6** only two mechanisms are possible, the loss of HCN, giving rise to the *m/z* 52.96 peak which corresponds to the $[Sr\text{-}OH_2]^{2+}$ ion in the MS/MS spectrum or its Coulomb explosion into $SrOH^+ + HCNH^+$, the partner peaks observed at *m/z* 104.90 and 28.02, via the **TS6A**.

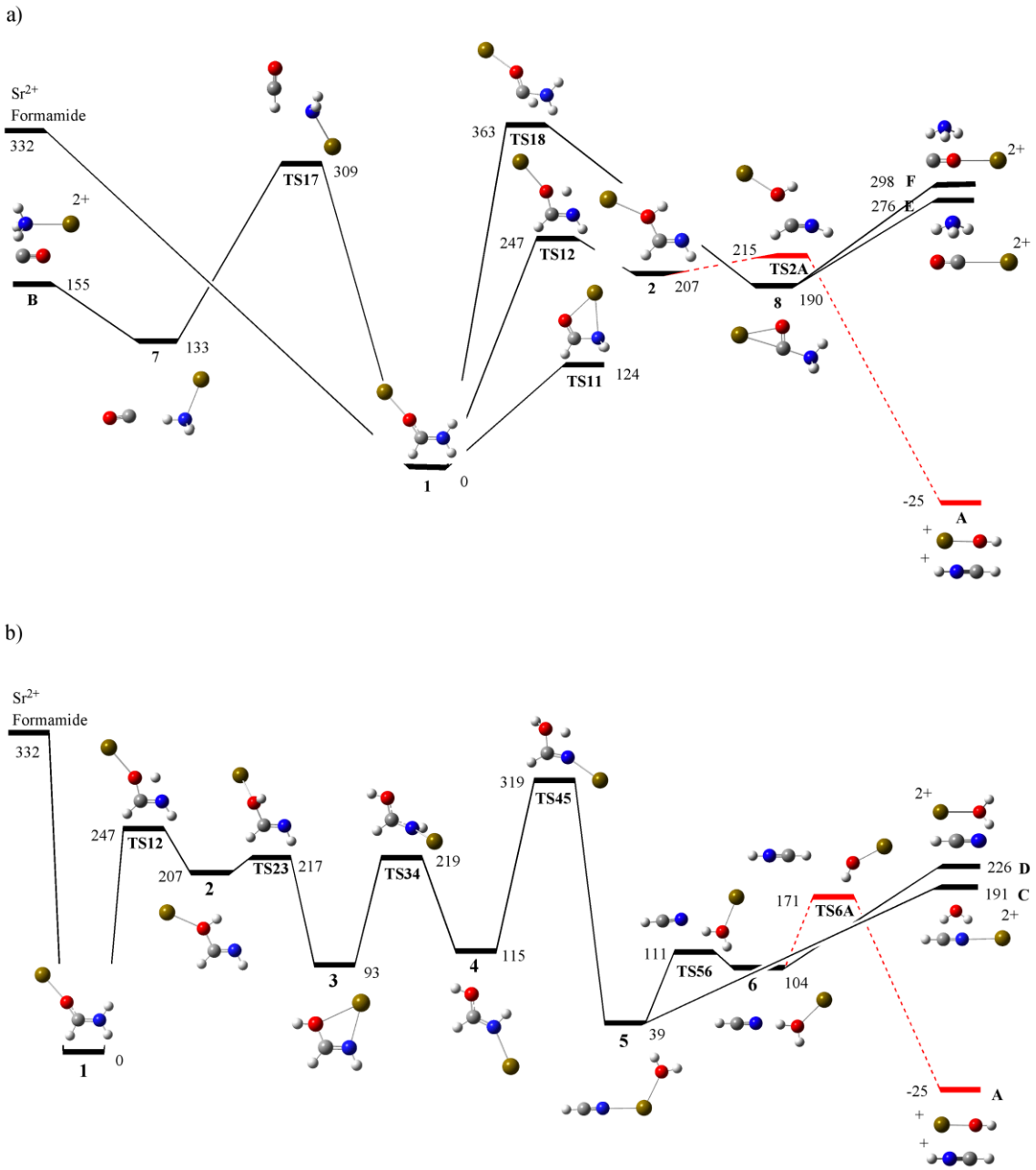

Figure 5. Schematic representation of the potential energy surfaces associated with the unimolecular reactions of the formamide-Sr^{2+} complexes with origin in the most stable adduct **1**. For the sake of clarity we have splitted the PES into two: (a) mechanisms involving the intermadiates **7** and **8** and the Coulomb explosion of **2** and (b) mechanisms through the intermediate **5** and the Coulomb explosion of **6**. Relative energies are in kJ mol^{-1}.

These potential energy profiles are also consistent with the minor loss of CO and of ammonia. From minimum **1**, two alternative proton transfer processes can be envisaged. The first one involves the cleavage of the C-N bond with a concomitant migration of the metal dication towards the amino group, through the transition structure **TS17**, which

lies at 309 kJ mol^{-1} above the global minimum **1**, and which gives rise to structure **7**. Minimum **7** undergoes the loss of CO leading to the *m/z* 52.46 peak in the MS/MS spectrum, which corresponds to $[NH_3\text{-}Sr]^{2+}$ doubly charged ion. This process is very unlikely to occur due to the high energy barrier connecting minimum **1** and minimum **7**, and is reflected in the low intensity of the peak corresponding to the ion $[NH_3\text{-}Sr]^{2+}$. The second proton transfer process corresponds to the migration of the proton from the C atom to the amino group via **TS18**, leading to minimum **8**. Structure **8** may directly lose NH_3 giving rise to **E** and **F** $[C,O,Sr]^{2+}$ fragments, depending on whether the metal attaches to the carbon atom or to the oxygen atom of carbon monoxide, respectively. The high barrier connecting minimum **1** with minimum **8**, which lies 31 kJ mol^{-1} above the entrance channel, make this process energetically unfavorable, and therefore the loss of ammonia should be hardly observable. This is in good agreement with the very low intensity observed for the $[C,O,Sr]^{2+}$ peak in the MS/MS spectra (see Figure 1). The height of the barrier for this proton transfer process is 62 kJ mol^{-1} higher in energy than that calculated for the isolated formamide, due to the decrease of the intrinsic basicity (enhanced acidity) of the amino group when formamide is attached to Sr^{2+}.

It is worth noting that one of the most intense peaks in the experimental spectrum corresponds to Sr^{2+}, which apparently should come from a dissociation into Sr^{2+} + formamide. This is similar to what has been previously observed in gas-phase reactions with Cu^+ or Ni^+. We cannot offer however a clear plausible explanation for this experimental finding, because, on the one hand, the formamide-Sr^{2+} binding energy is around 100 kJ mol^{-1} higher than the formamide-Cu^+ or formamide-Ni^+ ones, and on the other hand, practically all the mechanisms associated with the formation of the other observed products involve activation barriers which are below the entrance channel. One possible way, however, of producing the loss of Sr^{2+} would be the sequential fragmentation of complex **6**, by losing first a HCN molecule and then a water molecule,

since these process will be exothermic, which can be consistent, as indicated in previous sections, with the experimental observation.

Conclusions

The direct association of the Sr^{2+} with formamide gives rise to a unique complex **1** where the metal cation is attached to the carbonyl oxygen. No stable adducts with the metal ion attached to the amino group have been found, and the stationary point in which the metal bridges between both basic sites is a transition state which connects the global minimum with itself, in a process in which the metal cation orbits around the base.

The Sr^{2+} attachment to the formamide molecule significantly enhances the participation of the zwitterionic mesomeric structure **b**, through the conjugation of the nitrogen lone pair with the C=O π-system.

The unimolecular decomposition of collision-activated formamide-Sr^{2+} complexes leads the following ionic products, $[Sr\text{-}OH]^+$, $[HCNH]^+$, $[Sr\text{-}OH_2]^{2+}$, Sr^{2+}, $[Sr\text{-}NH_3]^{2+}$ and $[C,O,Sr]^{2+}$, the intensity of the two latter being very weak.

The topology of the calculated PES permits to establish the mechanisms which are associated with the aforementioned fragmentations. In these mechanisms structure **2**, in which the doubly charged metal ion is attached to the OH group of the enolic form of formamide, plays a crucial role, being the origin of the Coulomb explosion yielding $[Sr\text{-}OH]^+ + [HCNH]^+$, which is the dominant process.

Also, a multi-step mechanism with origin in **2**, involving two internal rotations and one 1,3H shift, leads finally to complex **6**, which loses HNC or alternatively undergoes a Coulomb explosion yielding again $[Sr\text{-}OH]^+ + [HCNH]^+$.

The strong peak corresponding to Sr^{2+} is still an open question, since it seems to be incompatible with the fact that all the aforementioned mechanisms involve activation

barriers which are below the entrance channel, the only possible mechanism being a sequential fragmentation of complex **6** by losing HCN and H_2O.

Sr^{2+} has an anti-catalytic effect on the enolic tautomerization of formamide, in contrast with the catalytic effect it exhibits when attached to uracil of its sulfur and selenium derivatives.[39]

Acknowledgments. This work has been partially supported by the DGI Project No. CTQ2009-13129-C01, by the Project MADRISOLAR2, Ref.: S2009PPQ/1533 of the Comunidad Autónoma de Madrid, by Consolider on Molecular Nanoscience CSC2007-00010, and by the COST Action CM0702. AE gratefully acknowledge a Ph.D grant from the Ministerio de Ciencia e Innovación of Spain. A generous allocation of computing time at the CCC of the UAM is also acknowledged.

Reference

1 H. Lavanant, E. Hecquet and Y. Hoppilliard, *Int. J. Mass Spectrom.*, 1999, **187**, 11-23.
2 G. Bhaskar, M. A. Chary, M. K. Kumar, K. Syamasundar, M. Vairamani and S. Prabhakar, *Rapid Communications in Mass Spectrometry*, 2005, **19**, 1536-1544.
3 S. Guillaumont, J. Tortajada, J. Y. Salpin and A. M. Lamsabhi, *Int. J. Mass Spectrom.*, 2005, **243**, 279-293.
4 F. R. Novara, H. Schwarz and D. Schroder, *Helv. Chim. Acta*, 2007, **90**, 2274-2280.
5 O. Mó, M. Yáñez, J. Y. Salpin and J. Tortajada, *Mass Spectrom. Rev.*, 2007, **26**, 474-516.
6 I. Corral, O. Mó, M. Yáñez, J. Y. Salpin, J. Tortajada and L. Radom, *J. Phys. Chem. A*, 2004, **108**, 10080-10088.
7 I. Corral, O. Mó, M. Yáñez, J. Y. Salpin, J. Tortajada, D. Moran and L. Radom, *Chem.-Eur. J.*, 2006, **12**, 6787-6796.
8 C. Trujillo, O. Mó, M. Yáñez, J. Y. Salpin and J. Tortajada, *ChemPhysChem*, 2007, **8**, 1330-1337.
9 M. F. Bush, J. Oomens, R. J. Saykally and E. R. Williams, *J. Am. Chem. Soc.*, 2008, **130**, 6463-6471.
10 C. Trujillo, O. Mó, M. Yáñez, J. Tortajada and J. Y. Salpin, *J. Phys. Chem. B*, 2008, **112**, 5479-5486.
11 R. C. Dunbar, A. C. Hopkinson, J. Oomens, C. K. Siu, K. W. M. Siu, J. D. Steill, U. H. Verkerk and J. F. Zhao, *J. Phys. Chem. B*, 2009, **113**, 10403-10408.

12 R. C. Dunbar, J. D. Steill, N. C. Polfer and J. Oomens, *J. Phys. Chem. B*, 2009, **113**, 10552-10554.
13 R. C. Dunbar, J. D. Steill and J. Oomens, *Phys. Chem. Chem. Phys.*, 2010, **12**, 13383-13393.
14 M. K. Drayss, P. B. Armentrout, J. Oomens and M. Schaefer, *Int. J. Mass Spectrom.*, 2010, **297**, 18-27.
15 H. Y. Lin, D. P. Ridge, E. Uggerud and T. Vulpius, *J. Am. Chem. Soc.*, 1994, **116**, 2996-3004.
16 A. Luna, B. Amekraz, J. P. Morizur, J. Tortajada, O. Mó and M. Yáñez, *J. Phys. Chem. A*, 2000, **104**, 3132-3141.
17 C. F. Rodriquez, X. Guo, T. Shoeib, A. C. Hopkinson and K. W. M. Siu, *J. Am. Soc. Mass Spectrom.*, 2000, **11**, 967-975.
18 J. I. Mujika, E. Formoso, J. M. Mercero and X. Lopez, *J. Phys. Chem. B*, 2006, **110**, 15000-15011.
19 S. Leach, H. W. Jochims and H. Baumgartel, *J. Phys. Chem. A*, 2010, **114**, 4847-4856.
20 U. Shanker, B. Bhushan, G. Bhattacharjee and Kamaluddin, *Astrobiology*, 2011, **11**, 225-233.
21 R. Saladino, C. Crestini, F. Ciciriello, G. Costanzo and E. Di Mauro, *Chem. Biodivers.*, 2007, **4**, 694-720.
22 J. Crovisier, *Astrobiology:Future Perspectives*, Kluwer/Springer, Dordrecht, 2004.
23 A. J. Markwick and S. B. Charnley, *Astrobiology:Future Perspectives*, Kluwer/Springer, Dordrecht, 2004.
24 T. J. Millar, *Astrobiology:Future Perspectives*, Kluwer/Springer, Dordrecht, 2004.
25 R. Saladino, C. Crestini, G. Costanzo and E. DiMauro, *Curr. Org. Chem.*, 2004, **8**, 1425-1443.
26 C. Reid, L. E. Orgel and Ponnampe.C, *Nature*, 1967, **216**, 936-&.
27 W. D. Fuller, L. E. Orgel and R. A. Sanchez, *J. Mol. Biol.*, 1972, **67**, 25.
28 E. A. Kuzicheva and N. V. Tsupkina, *Zhurnal Evolyutsionnoi Biokhimii i Fiziologii*, 1978, **14**, 213.
29 E. C. T. Kirk-Othmer, *Encyclopedia of Chemical Tecnology, Formic Acid and Derivatives (Formamide)*, Wiley Interscience, 1978.
30 X. C. Wang, J. Nichols, M. Feyereisen, M. Gutowski, J. Boatz, A. D. J. Haymet and J. Simons, *J. Phys. Chem.*, 1991, **95**, 10419-10424.
31 M. W. Wong, K. B. Wiberg and M. J. Frisch, *J. Am. Chem. Soc.*, 1992, **114**, 1645-1652.
32 H. B. Schlegel, P. Gund and E. M. Fluder, *J. Am. Chem. Soc.*, 1982, **104**, 5347-5351.
33 J. S. Kwiatkowski, R. J. Bartlett and W. B. Person, *J. Am. Chem. Soc.*, 1988, **110**, 2353-2358.
34 J. Tortajada, E. Leon, J. P. Morizur, A. Luna, M. O. and M. Yánez, *J. Phys. Chem.*, 1995, **99**, 13890-13898.
35 C. L. Perrin, *Accounts Chem. Res.*, 1989, **22**, 268-275.
36 S. Antonczak, M. F. Ruizlopez and J. L. Rivail, *J. Am. Chem. Soc.*, 1994, **116**, 3912-3921.
37 A. Luna, B. Amekraz, J. Tortajada, J. P. Morizur, M. Alcami, O. Mo and M. Yanez, *J. Am. Chem. Soc.*, 1998, **120**, 5411-5426.
38 L. Rodriguez-Santiago and J. Tortajada, *Int. J. Mass Spectrom.*, 2002, **219**, 429-443.
39 A. Eizaguirre, O. Mó, M. Yáñez and R. J. Boyd, *Org. Biomol. Chem.*, 2011, **9**,
.
40 G. Fogarasi and P. G. Szalay, *J. Phys. Chem. A*, 1997, **101**, 1400-1408.
41 P. Jayaweera, A. T. Blades, M. G. Ikonomou and P. Kebarle, *J. Am. Chem. Soc.*, 1990, **112**, 2452-2454.
42 P. M. W. Gill, *Mol. Phys.*, 1996, **89**, 433-445.
43 C. T. Lee, W. T. Yang and R. G. Parr, *Phys. Rev. B*, 1988, **37**, 785-789.

44 A. Eizaguirre, M. Yáñez, J. Tortajada and J. Y. Salpin, *Chem. Phys.Lett.*, 2008, **464**, 240-244.
45 S. F. Boys and F. Bernardi, *Mol. Phys.*, 1970, **19**, 553.
46 A. Luna, M. Alcamí, O. Mó and M. Yáñez, *Chem. Phys. Lett.*, 2000, **320**, 129-138.
47 A. Luna, M. Alcamí, O. Mó, M. Yáñez and J. Tortajada, *Int. J. Mass Spectrom.*, 2002, **217**, 119-129.
48 J. S. Lee, *J. Phys. Chem. A*, 2005, **109**, 11927-11932.
49 A. E. Shields and T. van Mourik, *J. Phys. Chem. A*, 2007, **111**, 13272-13277.
50 M. J. Frisch, G. W. Trucks, H. B. Schlegel, G. E. Scuseria, M. A. Robb, J. R. Cheeseman, J. Montgomery, J. A., T. Vreven, K. N. Kudin, J. C. Burant, J. M. Millam, S. S. Iyengar, J. Tomasi, V. Barone, B. Mennucci, M. Cossi, G. Scalmani, N. Rega, G. A. Petersson, H. Nakatsuji, M. Hada, M. Ehara, K. Toyota, R. Fukuda, J. Hasegawa, M. Ishida, T. Nakajima, Y. Honda, O. Kitao, H. Nakai, M. Klene, X. Li, J. E. Knox, H. P. Hratchian, J. B. Cross, V. Bakken, C. Adamo, J. Jaramillo, R. Gomperts, R. E. Stratmann, O. Yazyev, A. J. Austin, R. Cammi, C. Pomelli, J. W. Ochterski, P. Y. Ayala, K. Morokuma, G. A. Voth, P. Salvador, J. J. Dannenberg, V. G. Zakrzewski, S. Dapprich, A. D. Daniels, M. C. Strain, O. Farkas, D. K. Malick, A. D. Rabuck, K. Raghavachari, J. B. Foresman, J. V. Ortiz, Q. Cui, A. G. Baboul, S. Clifford, J. Cioslowski, B. B. Stefanov, G. Liu, A. Liashenko, P. Piskorz, I. Komaromi, R. L. Martin, D. J. Fox, T. Keith, M. A. Al-Laham, C. Y. Peng, A. Nanayakkara, M. Challacombe, P. M. W. Gill, B. Johnson, W. Chen, M. W. Wong, C. Gonzalez and J. A. Pople, Gaussian, Wallingford, CT, 2004.
51 R. F. W. Bader, *Atoms in Molecules. A Quantum theory*, Oxford, 1990.
52 C. F. Matta and R. J. Boyd, *The Quantum Theory of Atoms in Molecules*, Weinheim, 2007.
53 R. F. W. Bader and J. R. Cheeseman, AIMPAC Programs, 2000.
54 A. D. Becke and K. E. Edgecombe, *J. Chem. Phys.*, 1990, **92**, 5397-5403.
55 O. Mó, M. Yáñez, A. M. Pendas, J. E. Del Bene, I. Alkorta and J. Elguero, *Phys. Chem. Chem. Phys.*, 2007, **9**, 3970-3977.
56 S. Noury, X. Krokidis, F. Fuster and B. Silvi, *Comput. Chem.*, 1999, **23**, 597-604.
57 A. E. Reed, L. A. Curtiss and F. Weinhold, *Chem. Rev.*, 1988, **88**, 899-926.
58 A. J. Sadlej, *Collect. Czech. Chem. Commun.*, 1988, **53**, 1995-2016.
59 A. J. Sadlej, *Theor. Chim. Acta*, 1991, **79**, 123-140.
60 A. J. Sadlej and M. Urban, *Theochem-J. Mol. Struct.*, 1991, **80**, 147-171.
61 I. Cernusak, V. Kello and A. J. Sadlej, *Collect. Czech. Chem. Commun.*, 2003, **68**, 211-239.
62 E. D. Glendening, J. K. Badenhoop, A. E. Reed, J. E. Carpenter, J. A. Bohmann, C. M. Morales and F. Weinhold, NBO 5. G., Theoretical Chemistry Institute, University of Wisconsin, Madison, WI, 2004.
63 C. Trujillo, A. M. Lamsabhi, O. Mó and M. Yáñez, *Phys. Chem. Chem. Phys.*, 2008, **10**, 3229-3235.
64 J. Kohno, F. Mafune and T. Kondow, *J. Phys. Chem. A*, 1999, **103**, 1518-1522.
65 A. Irigoras, J. M. Mercero, I. Silanes and J. M. Ugalde, *J. Am. Chem. Soc.*, 2001, **123**, 5040-5043.
66 J. L. M. Abboud, I. Alkorta, J. Z. Davalos, J. F. Gal, M. Herreros, P. C. Maria, O. Mo, M. T. Molina, R. Notario and M. Yanez, *J. Am. Chem. Soc.*, 2000, **122**, 4451-4454.
67 C. Trujillo, A. M. Lamsabhi, O. Mo, M. Yanez and J. Y. Salpin, *Org. Biomol. Chem.*, 2008, **6**, 3695-3702.
68 A. M. Lamsabhi, O. Mo, M. Yanez and R. J. Boyd, *J. Chem. Theory Comput.*, 2008, **4**, 1002-1011.